ARTICLE   OPEN

Experimental evidence of exciton capture by mid-gap defects in CVD grown monolayer MoSe$_2$

Ke Chen[1], Rudresh Ghosh[2,3], Xianghai Meng[1], Anupam Roy[2,3], Joon-Seok Kim [2,3], Feng He[1,4], Sarah C. Mason[1], Xiaochuan Xu[5], Jung-Fu Lin[4,6,7], Deji Akinwande[2,3], Sanjay K. Banerjee[2,3] and Yaguo Wang[1,4]

In two dimensional (2D) transition metal dichalcogenides, defect-related processes can significantly affect carrier dynamics and transport properties. Using femtosecond degenerate pump-probe spectroscopy, exciton capture, and release by mid-gap defects have been observed in chemical vapor deposition (CVD) grown monolayer MoSe$_2$. The observed defect state filling shows a clear saturation at high exciton densities, from which the defect density is estimated to be around $0.5 \times 10^{12}/cm^2$. The exciton capture time extracted from experimental data is around ~ 1 ps, while the average fast and slow release times are 52 and 700 ps, respectively. The process of defect trapping excitons is found to exist uniquely in CVD grown samples, regardless of substrate and sample thickness. X-ray photoelectron spectroscopy measurements on CVD and exfoliated samples suggest that the oxygen-associated impurities could be responsible for the exciton trapping. Our results bring new insights to understand the role of defects in capturing and releasing excitons in 2D materials, and demonstrate an approach to estimate the defect density nondestructively, both of which will facilitate the design and application of optoelectronics devices based on CVD grown 2D transition metal dichalcogenides.

INTRODUCTION

Two-dimensional transition metal dichalcogenides (TMDs) have gained extensive research interests in recent years due to their extraordinary properties, such as direct band gap in monolayers,[1] strong spin-valley coupling,[2] and stable excitons or trions at room temperature.[3] These unique properties endow TMDs with many potential applications in electronics and photonics.[4] For example, the non-zero band gap provides a much higher on/off ratio in TMD-based field effect transistors than graphene-based ones.[5] The direct band gap in monolayer TMDs makes them excellent candidates for light-emitting diodes,[6] photodetectors,[7] and lasers.[8] The spin-valley coupling opens the possibility of realizing valleytronics, where the hole spin as a quantum information carrier can be manipulated through the interplay between spin and valley in spin quantum gates.[9]

Chemical vapor deposition (CVD) grown monolayer TMDs are known to have many defects caused by thermal strain and local variations in the precursor concentration during the growth process.[10] Defects can severely jeopardize the performance of TMD-based devices. For example, extremely low quantum efficiency (<0.6%) has been observed in static measurement of photoluminescence (PL) for prototypical MoS$_2$ due to non-radiative defect-associated recombination.[11] There are a number of defect types in TMDs, such as chalcogen atom vacancies, impurities, interstitials, antisite defects, and dislocations.[10] Some of the defects can induce mid-gap states, for example, the antisite defect,[12] chalcogen atom vacancy[13, 14] and nitrogen/oxygen impurities.[15] The mid-gap defects are believed to serve as either effective recombination centers or effective carrier traps, depending on whether the defects possess a small or large difference in capture rates of electrons and holes, respectively.[16]

Fundamental understanding of the role of defects in exciton/carrier dynamics in TMDs is essential to realize high-performance of TMD-based electronics. Recently, a number of ultrafast experiments [17–23] and a theoretical study[24] have been done to investigate the exciton/carrier dynamics in two-dimensional TMDs, suggesting significant influences of defects on the exciton/carrier recombination dynamics. In these previous experiments,[17–24] exciton/carrier dynamics were detected by resonant probe or terahertz probe, and the interactions between exciton/carrier and defects were indirectly inferred from exciton/carrier population decay. One general observation of the previous studies is that the relaxation of photoexcited carriers/excitons shows a fast, few picoseconds decay followed by a slow several tens of picoseconds component. The fast decay can be due to Auger recombination through some mid-gap defects in exfoliated TMDs, which act as effective recombination centers capturing most of the excited electrons and holes simultaneously within 1–2 ps.[17] Defect trapping excitons/carriers is another possible reason for the fast decay.[22, 23] However, very little was known about the role of mid-gap defects serving as carrier traps in 2D TMDs. Even though defect trapping carriers has been found as the origin of the hysteresis phenomenon in electrical I_{DS}–V_G measurement of TMD field effect transistors,[25] still, not any spectroscopic signal has been assigned as a direct defect trapping signature in time-resolved transient optical measurements.

[1]Department of Mechanical Engineering, The University of Texas at Austin, Austin, TX 78712, USA; [2]Microelectronics Research Center, The University of Texas at Austin, Austin, TX 78758, USA; [3]Department of Electrical and Computer Engineering, The University of Texas at Austin, Austin, TX 78758, USA; [4]Texas Materials Institute, The University of Texas at Austin, Austin, TX 78712, USA; [5]Omega Optics, Inc., Austin, TX 78757, USA; [6]Department of Geological Sciences, Jackson School of Geosciences, The University of Texas at Austin, Austin, TX 78712, USA and [7]Center for High Pressure Science and Technology Advanced Research (HPSTAR), 201900 Shanghai, China
Correspondence: Yaguo. Wang (yaguo.wang@austin.utexas.edu)

npj
Applications of optoelectronics-based on CVD
Ke Chen et al.

2

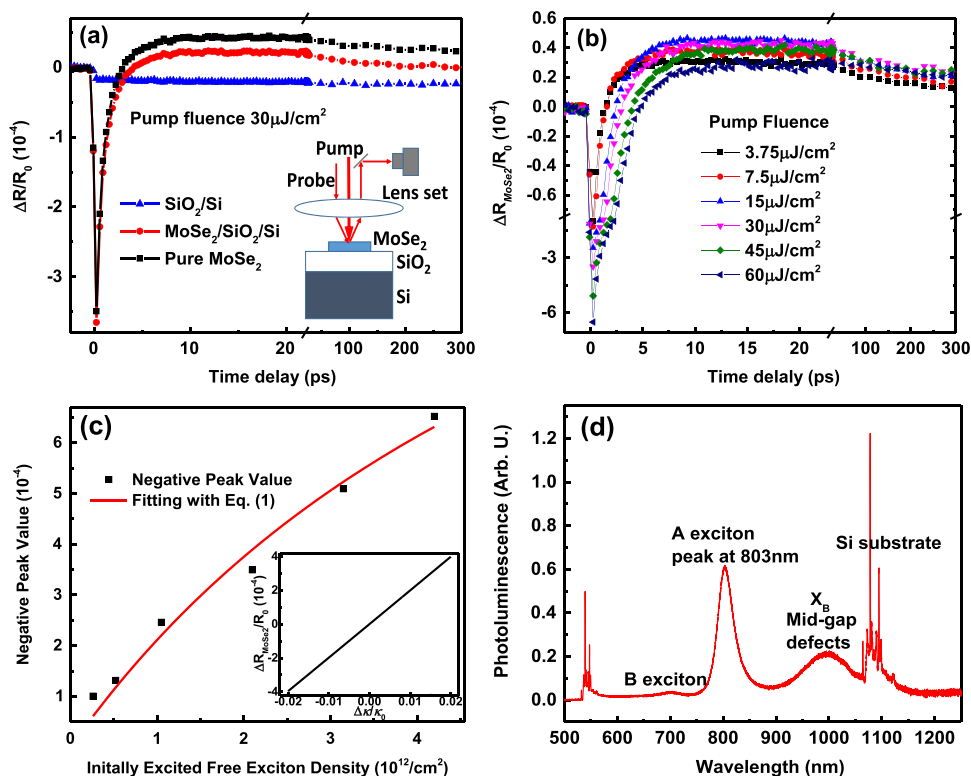**Fig. 1** **a** Differential reflection signals, $\Delta R/R_0$, measured at pump fluence of 30 µJ/cm^2, for both SiO$_2$/Si and MoSe$_2$/SiO$_2$/Si structures. The *black squares* represent the extracted signal of pure MoSe$_2$. *Inset*: sample structure and pump-probe detection geometry. **b** The extracted signals of pure monolayer MoSe$_2$ at various pump fluences. **c** Absolute values of the negative peak of signals in Fig. 1b and the fitting with the saturable absorption model (Eq. 1). *Inset*: Simulation of $\Delta R_{MoSe_2}/R_0$ vs. $(\Delta \kappa / \kappa_0)_{MoSe_2}$, using the transfer matrix method. **d** Photoluminescence signal of CVD monolayer MoSe$_2$ under 532 nm excitation measured at room-temperature in air

Here, we used degenerate pump-probe spectroscopy to study defect-related exciton dynamics in CVD grown monolayer MoSe$_2$. By tuning the wavelengths resonant with the A exciton, we observed an unexpected rapid sign change followed by a slow decay in the transient reflection signal, which can be viewed as ultrafast optical signature of defect capturing and trapping excitons. The defect trapping feature is further demonstrated by the phenomenon of the saturation of defect state filling. Based on the large difference between the fast capture time and the slow release time we obtained, it is found that some mid-gap defect in CVD grown TMDs can serve as an effective carrier trap rather than a recombination center as previously discovered in exfoliated TMDs.

RESULTS

Time resolved differential reflectivity signals of our CVD grown monolayer MoSe$_2$ sample synthesized on a SiO$_2$(285 nm)/Si substrate and the bare SiO$_2$(285 nm)/Si substrate at pump fluence of 20 µJ/cm^2 are shown in Fig. 1a. The differential reflectivity is defined as the relative change of reflection (ΔR) with respect to static reflectivity (R_0): $\Delta R/R_0 = (R - R_0)/R_0$. The signal from the SiO$_2$/Si substrate has a substantial contribution to the overall optical response in the MoSe$_2$/SiO$_2$/Si sample. To analyze the ultrafast dynamics purely from the monolayer MoSe$_2$, contributions from the substrate must be eliminated first. With the transfer-matrix method,[26] it is found that for a small perturbation of refractive index, the total reflection change of the MoSe$_2$/SiO$_2$/Si system is just a linear superposition of the contributions from MoSe$_2$ and Si, i.e., $\Delta R_{total} = \Delta R_{MoSe_2} + \Delta R_{Si}$ (See supplementary information for details). The contribution from SiO$_2$ is not considered because SiO$_2$ is non-absorptive at 800 nm. Therefore, the pure optical response

of MoSe$_2$ can be obtained by subtracting the optical response of Si (*blue triangles* in Fig. 1a) from the total response of MoSe$_2$/SiO$_2$/Si (*red dots* in Fig. 1a), shown as *black squares* in Fig. 1a.

The differential reflectivity signals purely from MoSe$_2$ ($\Delta R_{MoSe_2}/R_0$) at various pump fluences are shown in Fig. 1b. All signals show first a negative sharp peak and then a positive peak, followed by a slow decay. Reflectivity change of the probe can come from either the real part (n) or the imaginary part (κ) of the refractive index: $\tilde{n} = n - i\kappa$ (Note that positive κ stands for absorption). When the probe photon energy is resonant with or smaller than the exciton state, the pump-induced absorption change of the probe (change in the imaginary part) dominates the optical response.[17, 18, 27] Using the reflectivity formula for the TMDs/SiO$_2$/Si structure (see Eq. 1 in supplementary information), the change of reflectivity $\Delta R_{MoSe_2}/R_0$ due to small perturbations of the imaginary part of refractive index $(\Delta \kappa / \kappa)_{MoSe_2}$ has been calculated (Inset of Fig. 1c). It can be seen that $\Delta R_{MoSe_2}/R_0$ is almost linearly proportional to $(\Delta \kappa / \kappa)_{MoSe_2}$. Hence, the initial decrease and then increase of the reflectivity change observed in Fig. 1b corresponds to first a decrease and then an increase of the absorption for the probe, respectively. The sharp negative peaks shown in Fig. 1b are not artifacts from pump-probe correlation, which has been minimized by setting the polarizations of the pump and probe beams perpendicular to each other. Moreover, the full width at half maximum of the negative peaks is about several picoseconds, much longer than the laser pulse width. Considering that our laser wavelength (800 nm) is resonant with A exciton energy state (see the PL data in Fig. 1d), the sharp negative peaks can be related to phase-space filling effect at the A exciton state of MoSe$_2$, as illustrated in Fig. 2a. The phase-space filling effect comes from Pauli repulsion where an electron (hole) in existing exciton occupies the available phase space and
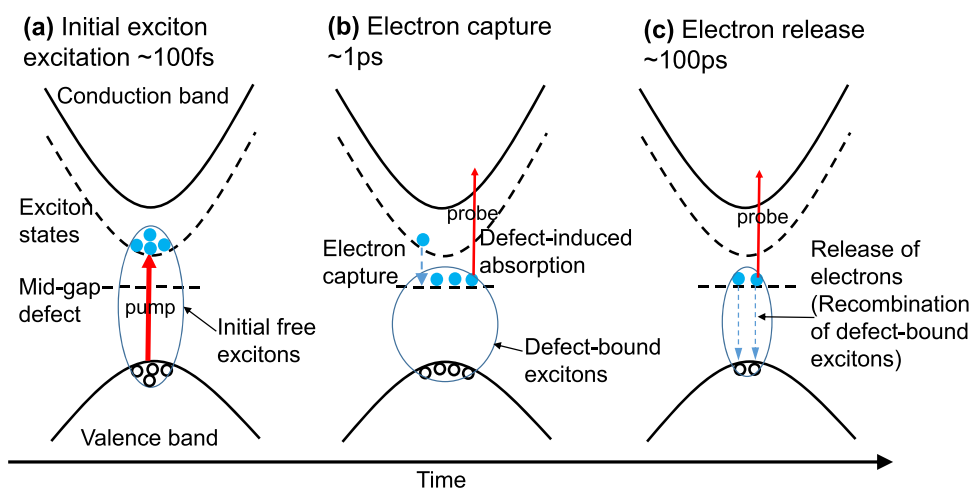
Fig. 2 Schematic of the dynamics of mid-gap defects capturing and releasing photoexcited electrons in MoSe$_2$. **a** Initial free exciton generation by the resonant pump laser pulse. **b** The excited electrons being captured by the mid-gap defects, after which the transitions from defect states to high energy states in the conduction band become available and increase the absorption of the probe. **c** The trapped electrons being released by the mid-gap defects and back to the valence band

suppresses the transition from optical absorption that forms the same exciton.[28] Therefore, the pump-generated A excitons can decrease the absorption of the probe light which is resonant with the A exciton state. Assuming one absorbed pump photon generates one exciton, the density of the pump-generated excitons (N) can be determined by the product of pump fluence and the absorbance of the MoSe$_2$ layer A_0 (1.74%, calculated with transfer matrix method, see supplementary for details). Due to the existence of pump-generated excitons, i.e., the phase-space filling effect, the absorption of the probe is governed by the saturable absorption model, according to which the nonlinear optical absorption coefficient α can be expressed as[29]: $\alpha = \alpha_0/(1 + N/N_s)$, where α_0 is the linear absorption coefficient and N_s is the saturation exciton density. Because the differential reflection of the probe is proportional to the change of the imaginary part of refractive index $\Delta\kappa$ (the change of the absorption coefficient $\Delta\alpha$, see inset of Fig. 1c), the amplitude of the negative peak can be expressed as:

$$\frac{\Delta R}{R_0} = C\frac{\Delta\alpha}{\alpha_0} = C\frac{N}{N + N_s} \qquad (1)$$

where C is a scaling constant. Plotted in Fig. 1c are absolute values of the negative peaks as a function of the free initial exciton density N generated by pump. Fitting of the data with Eq. (1) yields a saturation exciton density $N_s \sim 6.9 \times 10^{12}/\text{cm}^2$, which agrees well with the value $(5.8 \pm 0.5) \times 10^{12}/\text{cm}^2$ reported in Ref. 30 This agreement confirms that the negative peak comes from the phase-space filling effect at the A exciton state.

DISCUSSION

The remarkable observation is that the negative peak decays quickly and then even flips to positive. Such sign change has not been seen in exfoliated TMDs when the probe wavelength was also set resonant with the exciton state of 2D TMDs.[20, 30, 31] The rapid change of $\Delta R_{\text{MoSe}_2}/R_0$ signal from negative to positive indicates that the initially generated free excitons, which can decrease the absorption, quickly vanish, and then an absorption increase occurs. In traditional semiconductors and 2D material graphene, mechanisms such as bandgap renormalization (BGR)[32, 33] and free carrier absorption (FCA)[17] can be responsible for the pump-induced absorption increase. However, both BGR and FCA can be ruled out in our experiment for several reasons: BGR should cause a red-shift of the absorption spectrum of the probe. This

shift should lead to a reduced absorption rather than an increased absorption because the probe wavelength is set to resonant with the A exciton absorption peak. Even if BGR plays a role at short time delay through many-body interactions among electrons and holes generated by the pump, it should vanish quickly at low density ($<3 \times 10^{11}/\text{cm}^2$).[34] As the electron/hole densities decrease with time, exciton phase-space filling effect should re-dominate and the signal $\Delta R_{\text{MoSe}_2}/R_0$ should quickly drop back to negative values, which is not seen in the whole range of time delay. The probability of FCA is expected to be much lower than that of the phase-space filling effect, because the FCA needs assistance from phonons to satisfy momentum conservation, while the phase-space filling effect in our monolayer sample involves direct bandgap transition which does not require phonons. Dark exciton is an important consideration in understanding the exciton dynamics in monolayer TMDs.[35] However, the formation of dark exciton can only influence the population (magnitude) of the detectable bright exciton, but cannot flip the sign of the transient signal. Spectral broadening effect due to the exciton-exciton interaction is another possible reason that can lead to absorption increase and sign change in transient signal.[19, 36] Spectral broadening leading to absorption increase could appear with off-resonant probe, especially when the probe energy lies between A and B excitons or at the edges of absorption peak. However, at resonant probe position, spectral broadening instead leads to absorption decrease. As a result, spectral broadening should not be responsible for an increased absorption here when laser wavelength is set resonant with A exciton. Furthermore, the feature of a negative-to-positive sign change holds over a wide range (790–820 nm) around the A exciton resonance (803 nm, 1.55 eV) (Fig. S3 in supplementary information), which confirms that the transient $\Delta R_{\text{MoSe}_2}/R_0$ signal reflects the formation and fast vanish of A exciton, and is not a result of spectral broadening.

Another mechanism that can induce absorption increase is the absorption of the probe by the defect-captured electrons/holes, as shown in Fig. 2b (Note that only electron capture is shown for simplicity). In this mechanism, some defects, especially the mid-gap defects, can serve as electron/hole traps which quickly capture the electrons/holes generated by the pump laser. Once the mid-gap defect states are occupied by carriers, an additional absorption path becomes available. A probe photon can excite electron/hole from defect states to the conduction (electron)/valence (hole) band, and hence, the absorption of the probe increases. This mechanism can be very efficient in materials with a
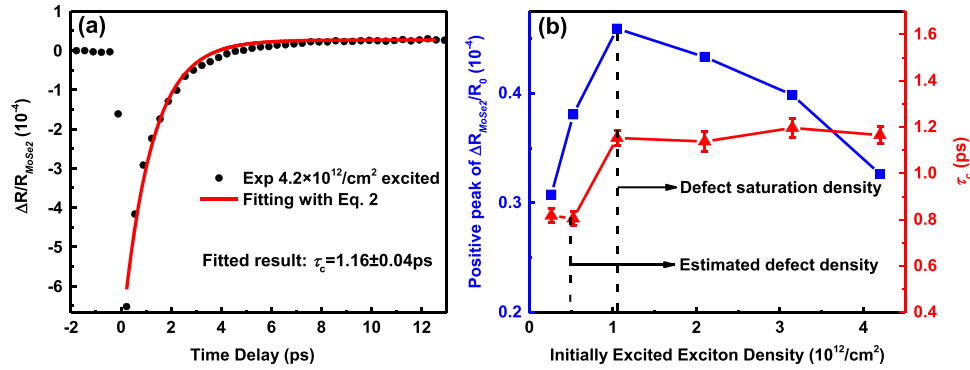
Fig. 3 **a** Fitting of defect capturing time using Eq. (2), with data measured at exciton density of $4.2 \times 10^{12}/cm^2$ (60 µJ/cm^2). **b** Positive peak values and the fitted defect capturing time as a function of free exciton density

considerable amount of defects. In low-temperature grown (LTG) traditional semiconductors, where abundant mid-gap point defects are created intentionally, such as LTG-GaAs,[37, 38] LTG-InP,[39] and LTG-InGaP,[40] a sign change in the differential transmission or reflection signals is well considered as a signature of transition from initial absorption bleaching to defect-capturing-induced absorption. CVD grown monolayer TMDs are known to contain many mid-gap defects,[10] such as chalcogen atom vacancy,[13, 14] antisite defect Mo_S and Mo_{S2},[12] and nitrogen/oxygen impurities.[15] The existence of the mid-gap defects in our CVD $MoSe_2$ sample is manifested by a broad peak around 1000 nm (1.25 eV) in the PL data, which is measured under ambient condition (Fig. 1d). Similar PL peaks (X_B peaks) have also been observed for mid-gap defects in ion beam-irradiated exfoliated TMDs [15, 41, 42] and as grown CVD MoS_2,[43] which are associated with chalcogen atom vacancies (or impurity atoms occupying the vacancies) induced by the ion beam or during the growth process due to high volatility of chalcogenides, with energy level 0.1–0.3 eV above the valence band maximum or below the conduction band minimum. The defect peak shown in our PL data not only indicates a rich source of mid-gap defects in the CVD grown $MoSe_2$ sample, but also confirms the ability of the mid-gap defect to rapidly capture the photoexcited excitons and assist their radiative recombination process. Therefore, it is very reasonable to attribute the rapid transition from negative peak to positive peak (probe absorption increase) in $\Delta R_{MoSe_2}/R_0$ signal to the process of defect states capturing excitons. When an electron or hole is trapped, the whole exciton is actually trapped to form a defect-bound exciton (X_B).[15, 44] The slow decay after positive peak is associated with defect release of the trapped electrons/holes to the valence/conduction band, equivalently, the recombination of defect-bound excitons, as shown in Fig. 2c.

The capture of excitons by defects (from negative peak to positive peak) can be described with a simple exponential decay:

$$\Delta R(t) = \Delta R_{pos} + \left(\Delta R_{neg} - \Delta R_{pos}\right)\exp(-t/\tau_c) \qquad (2)$$

where ΔR_{pos}, ΔR_{neg}, and τ_c are the positive peak value, the negative peak value, and the capture time, respectively. Fig. 3a plots the fitting with Eq. (2) at a free exciton density of $4.2 \times 10^{12}/cm^2$ (60 µJ/cm^2). Fig. 3b plots the positive peak values ΔR_{pos} and the fitted τ_c as a function of initial free exciton density. Interestingly, the positive peak values firstly increase with exciton density and then decrease after a threshold value of the exciton density. This phenomenon is an exact demonstration of the saturation of defect states filling, further confirming the defect trapping feature of the observed exciton dynamics. Before the saturation of defect states, increasing exciton density will result in an increase of the filled defect states, hence the increase of positive peaks. Once defect states are saturated, or in other words, after all the defect states are occupied, further increase of excitation density will cause an

increased population of excess excitons and enhanced exciton phase-filling effect, which contributes negatively to the $\Delta R_{MoSe_2}/R_0$ signal. Therefore, positive peak values decrease after the saturation of defect states. In previous static PL studies, the saturation of defect state filling has also been indicated by the nonlinear saturable dependence of defect PL (X_B) intensity on the excitation fluence.[42, 44] Note that the surviving excess exciton density is not just the injected exciton density minus the trapping defect density, because besides the trap-like defects, there are also fast-recombination-center-like defects. With these recombination centers, exciton recombination can occur within picoseconds timescale through the defect-assisted Auger process.[17] Therefore, defect-assisted exciton trapping and fast recombination actually take place simultaneously, which means most of the excess excitons have already recombined after the trap-like defects saturate, leaving only a few surviving excess excitons. In Fig. 3b, ΔR_{pos} starts to decrease at exciton density of $1.04 \times 10^{12}/cm^2$, indicating that the trap defect density starts to saturate. Since the defect-assisted fast recombination time (1–2 ps)[17] is on the same order as the exciton capture time τ_c (will be shown later), it is reasonable to assume that the amounts of the fast recombined excitons and the captured but trapped ones are on the same order. Therefore, the trap-like defect density in monolayer $MoSe_2$ is estimated to be around $0.5 \times 10^{12}/cm^2$. The value obtained here is consistent with the reported values in monolayer MoS_2 samples: $0.3 \times 10^{12}/cm^2$ from fitting of the transient transmission change $\Delta T/T_0$ for the density of fast carrier-capture defects,[17] and $10^{12}/cm^2$ from a scanning tunneling microscopy measurement[45] for point defect density.

The magnitudes of the fitted τ_c shown in Fig. 3b are about 0.8–1.2 ps, which agree well with the result of 600 fs charge trapping time obtained from a transient photoconductivity measurement in CVD grown MoS_2[22] and a recent theoretical work predicting that the defect capturing exciton time in TMDs can range from less than a picosecond to a few picoseconds.[24] The τ_c reveal a step-like increase around the defect-saturation exciton density ($1.04 \times 10^{12}/cm^2$), which confirms the saturable manner of exciton capture by defects. When the initially excited exciton density is much lower than the defect density, defect capturing functions at its full capacity and the capture occurs quickly. When the initially excited exciton density is close to or higher than the defect density, defect states become full and the capture becomes slower.

As mentioned earlier, the decay of the positive signal shown in Fig. 1b is associated with defects releasing the trapped excitons. Fig. 4a plots the $\Delta R_{MoSe_2}/R_0$ signals normalized at positive peaks. The decay signals can be well fitted by two exponential functions:

$$\left(\frac{\Delta R}{R_0}\right)_{normalized} = A_1 \exp\left(-\frac{t}{\tau_1}\right) + A_2 \exp\left(-\frac{t}{\tau_2}\right), \qquad (3)$$
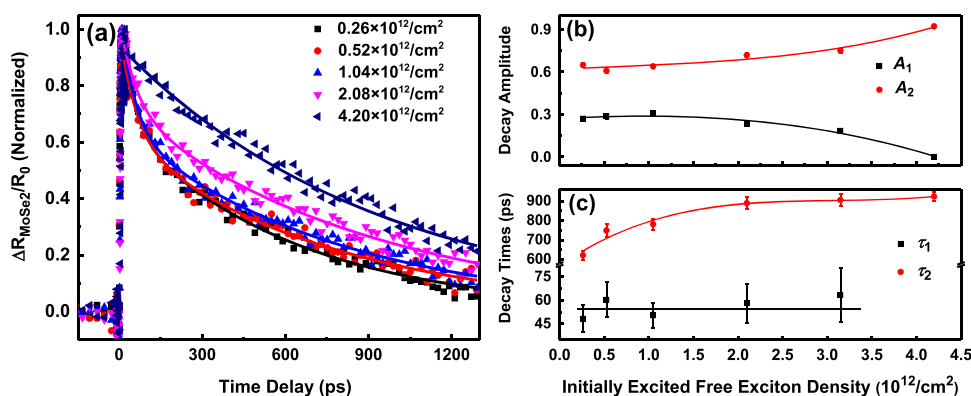
Fig. 4 **a** Differential reflectivity signal of $MoSe_2$ normalized at positive peaks. The *solid curves* are fittings using Eq. 3. **b** The fitted decay amplitudes and **c** the fitted decay times vs. free exciton density. The *solid lines* are guides for the eye

where A_1, τ_1 and A_2, τ_2 represent the amplitudes and decay times of the fast and slow decay components, respectively. Fig. 4b and c plot the fitted amplitudes and decays times, respectively, as a function of initial free exciton density. When the injected exciton density is higher than $1.04 \times 10^{12}/cm^2$, the defect traps are saturated, leaving a certain amount of surviving excess excitons. Thus only the first three data points taken below $1.04 \times 10^{12}/cm^2$ purely reflect the exciton releasing dynamics. This is confirmed by the fact that these three data points almost overlap after normalization (Fig. 4a). The average fast and slow decay times are around 52 and 700 ps, respectively. One possible explanation is that the fast and slow decay corresponds to the release of holes and the release of electrons, respectively. Because monolayer $MoSe_2$ is natively n-doped[46] with more intrinsic electrons than holes, due to the imbalance of electron and hole amounts, it is easier to release a bound hole from a hole-trapping defect (equivalent to capturing a free electron by the hole-trapping defect), than to release a bound electron from an electron-trapping defect (equivalent to capturing a free hole by the electron-trapping defect). Amplitudes A_1 and A_2 in Eq. (3) represent the proportions of the hole-trapping defect and the electron-trapping defect[47] in the sample, respectively. When the initially injected exciton density is larger than $1.04 \times 10^{12}/cm^2$, the A_1(fast) decay component becomes smaller with increasing exciton density (See Fig. 4b). Since population of hole-trapping defect (A_1 component) does not change, the decrease of A_1 is an artificial effect from excess excitons. The excess excitons contribute a negative decay to the $\Delta R_{MoSe_2}/R_0$ signal and have a defected-assisted slow recombination time (tens of picoseconds)[17] comparable to τ_1 (the decay time of A_1 component), Therefore, the negative-signed excess excitons compensate the positive-signed A_1 component of trapped exciton, and increasing of excess excitons gives the apparent decreasing trend of A_1 component.

To investigate the effects on defect capturing signature from substrate, sample thickness, and synthesis method, we have further measured the exciton/carrier dynamics in three more samples: CVD grown monolayer $MoSe_2$ transferred onto quartz substrate, CVD grown ~10-layer $MoSe_2$ on SiO_2/Si substrate (thickness estimated from $\Delta R/R_0$ peak signal), and exfoliated 40-layer $MoSe_2$ on SiO_2/Si substrate (Fig. S4), using the same experimental setup. Fig. 5a and b show the transient $\Delta R/R_0$ and $\Delta T/T_0$ signals of CVD grown monolayer $MoSe_2$ on quartz. Theoretically, $\Delta R = R - R_0$ of a thin film on a transparent substrate is proportional to the change of absorbance $\Delta A = A - A_0$ (where A and A_0 are absorbance with and without pump, respectively),[20] while $\Delta T/T_0$ signal of TMDs on transparent substrate is negatively proportional to the change of absorbance ΔA.[17] Results shown in Fig. 5a and b have three important implications: i) defect

capturing exciton phenomenon is independent on substrate, because the same spectroscopic signature of defect capturing exciton still exist in CVD grown sample on quartz substrate. This result shows that the trapping defects is an intrinsic property of the sample but not from substrate effect. ii) The good symmetrical feature between $\Delta R/R_0$ and $\Delta T/T_0$ signals agrees with the above theoretical prediction, confirming that the optical response of an excited $MoSe_2$ sample probed resonantly is indeed dominated by the absorption change. iii) The positive (negative) peak of $\Delta R/R_0$ ($\Delta T/T_0$) starts to decrease (increase) at pump fluence of 42 μJ/cm² ($4.4 \times 10^{12}/cm^2$ injected exciton), from which the trapping defect density in the transferred sample is estimated to be around $2.2 \times 10^{12}/cm^2$. This value is a little higher than that in the un-transferred sample (Fig. 3b), which is attributed to the additional defects introduced during the transfer process.

Figure 5c shows the pure $\Delta R/R_0$ signal of the CVD grown multilayer $MoSe_2$ on SiO_2/Si with the Si contribution removed. The signature of defect capturing exciton, a first negative peak and then a quick following positive platform, can still be seen. Using the transfer matrix method, we calculate the absorbance of the sample (0.1442), and estimate that $1 μJ/cm^2$ pump fluence corresponds to an excited carrier density of $5.8 \times 10^{10}/cm^2$ per layer (see supplementary information for details). Fig. 5c shows that the positive peak value of the signals roughly starts to decrease at pump fluence around 9.6 μJ/cm², corresponding to an excited carrier density about $5.6 \times 10^{11}/cm^2$ per layer. This indicates a trapping defect density of $0.28 \times 10^{12}/cm^2$, on the same order but a little smaller than the estimated trapping defect density ($0.5 \times 10^{12}/cm^2$) in monolayer CVD $MoSe_2$. Such difference in defect density between CVD multilayer and monolayer samples is reasonable, because 1) thicker multilayer sample should have a better Se atom deposition hence fewer Se vacancy defects, and 2) thicker sample should have fewer inner defects due to protection by the top layers. Fig. 5d shows $\Delta R/R_0$ of the exfoliated 40-layer $MoSe_2$ sample on SiO_2/Si substrate. Consistent with the literature results,[20, 30, 31] our measured transient signal on exfoliated $MoSe_2$ only shows one-sign (negative) exponential decay, revealing only carrier recombination through the phase filling effect. The fact that no sign change is observed in exfoliated $MoSe_2$ indicates that either the defects in the exfoliated sample can only work as recombination centers, or the trapping defect amount is much fewer than that of the CVD sample. Thus far, we found that the spectroscopic sign-changing signature of defect trapping exciton/carriers is unique to CVD grown sample.

We have also performed a surface cleaning treatment on the CVD monolayer sample to remove any possible surface adsorbates, after which immediately re-measure the $\Delta R/R_0$ signal (see supplementary information). No change has been observed in the $\Delta R/R_0$ signal after the cleaning, indicating that the sign-

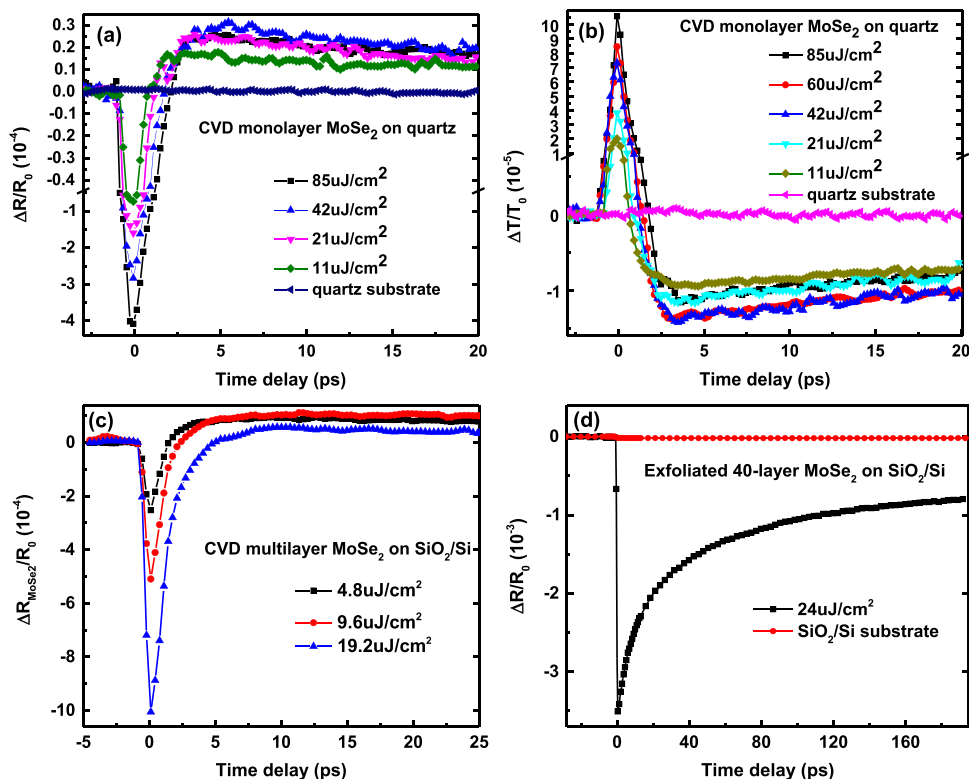**Fig. 5** **a** and **b** Differential reflection and transmission signals of a CVD grown monolayer $MoSe_2$ on quartz substrate. **c** Differential reflection signals of a CVD grown 10-layer $MoSe_2$ on SiO_2/Si substrate. **d** Differential reflection signal of an exfoliated 40-layer $MoSe_2$ on SiO_2/Si substrate

changing feature of $\Delta R/R_0$ is not due to the physical adsorbates such as gas molecules and particles, which are weakly bonded to the surface and easy to clean or remove even with femtosecond laser pulses.[48] In order to reveal the nature of the possible trapping defects, we have performed X-ray Photoelectron Spectroscopy (XPS) measurements on the CVD monolayer and exfoliated multilayer samples (Fig. 6). The measured Mo $3d_{5/2}$ (Se $3d_{5/2}$) peak position is at around 228.5 (54) eV, which are consistent with the literature values.[49, 50] Also shown are the Gaussian–Lorentzian fittings to the 3d peaks. From the area ratio of $3d_{5/2}$ peaks, we can get the composition ratio of Mo:Se: about 1:1.87 in exfoliated sample and about 1:1.82 in CVD sample. For both samples, the Se: Mo ratio are less than the nominal value of 2:1, indicating the presence of a large amount of chalcogen vacancies in both samples. These results indicate that the Se vacancy may not be the responsible trapping defect since it appears massively in both samples. Another remarkable observation is that two peaks locating at 235.5 and 58.5 eV only appear in the CVD sample, but not in the exfoliated one. These two peaks are the Mo-oxide and Se-oxide peaks, respectively.[51, 52] The strong oxide peaks are clear evidence of a rich source of the oxygen-related defects, such as substitutional oxygen impurity, Mo–O bonds and Se–O bonds, existing in the CVD sample. The difference in oxygen content between CVD and exfoliated samples can arise from the CVD growth process, because during the growth a large number of Se vacancies and boundary edge sites are present in the sample, and these vacancies and edge sites, generally, are highly reactive to the oxygen atoms generated from the MoO_3 precursor in the chamber, so O impurity will form inevitably in the growth process.[53] Considering the fact that O impurity only appears in CVD sample while Se vacancy can be found in both, and that the sign change of $\Delta R/R_0$ is only observed in CVD sample, we conclude that the oxygen-associated impurities introduced during

the CVD growth process due to the existence of Se vacancies and edge sites could play an important role in exciton trapping.

In summary, femtosecond pump-probe spectroscopy has been used to investigate defect capturing and releasing excitons in CVD grown $MoSe_2$ samples. Ultrafast reflectivity signals of monolayer $MoSe_2$ show initially negative and then positive peaks, followed by slow decays. The observed phenomenon is a strong evidence of mid-gap defect capturing and releasing the excited excitons. The existence of mid-gap defects and their ability to capture photoexcited carriers has been confirmed by the PL data. From the defect filling saturation, the defect density has been estimated to be around 0.5×10^{12}/cm^2 in CVD grown monolayer $MoSe_2$. The experimentally acquired value for exciton capture time, as well as average fast and slow release times, are about 1, 52, and 700 ps, respectively. Since $MoSe_2$ is naturally n-doped, the fast and slow release processes are attributed to the release of holes and electrons, respectively. The defect capturing and trapping of excitons presents in all CVD grown samples, regardless of substrate and sample thickness. Our results unveil the carrier-trapping role of defects in CVD grown $MoSe_2$, which is very important to understand the defect-related carrier dynamics in TMDs and will facilitate the design and application of high-speed optoelectronics devices based on CVD grown 2D TMDs. XPS measurements suggest that the oxygen-associated impurities could serve as the exciton/carrier trappers.

METHODS

Sample synthesis and preparation

Monolayer $MoSe_2$ and the ~10layer-thick $MoSe_2$ were synthesized on a SiO_2 (285 nm)/Si substrate by chemical vapor deposition with MoO_3 powder and Diethyl Selenide. Details of the growth process have been explained in Ref. 54 The monolayer thickness has been confirmed by PL spectroscopy and atomic force microscopy measurement.[54] To study the
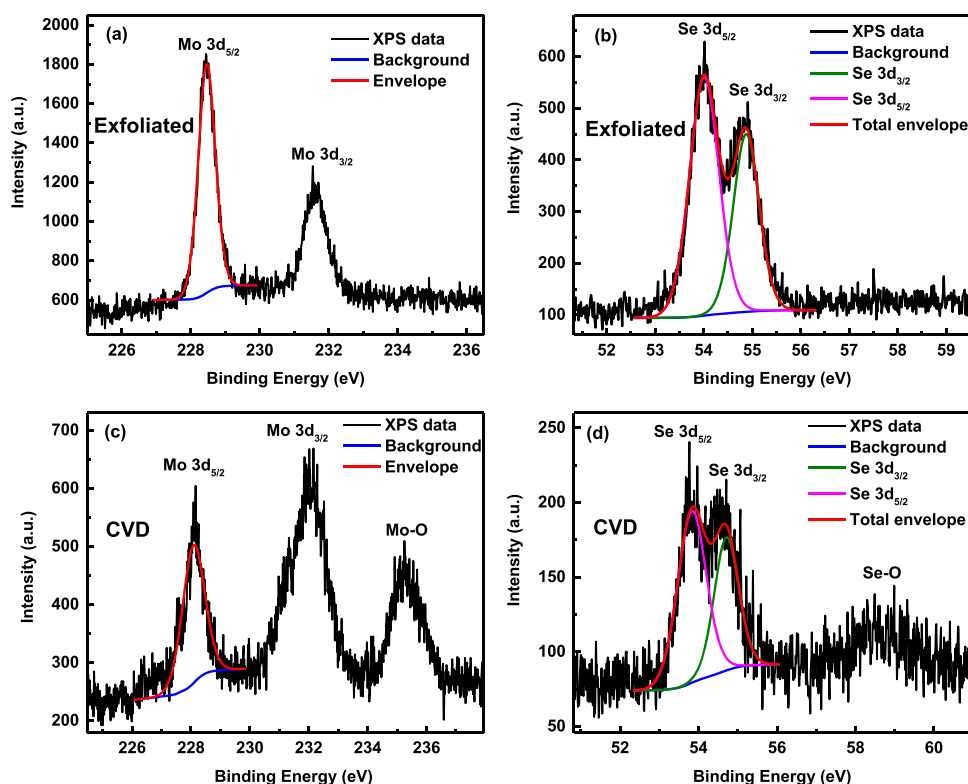
Fig. 6 X-ray Photoelectron Spectroscopy results of the exfoliated multilayer and CVD monolayer MoSe$_2$ samples: **a** and **c** are the Mo 3d peaks in exfoliated and CVD samples, respectively; **b** and **d** are the Se 3d peaks in exfoliated and CVD samples, respectively

effects of substrates, part of the CVD grown monolayer MoSe$_2$ was transferred onto a quartz substrate. The ~40 layer-thick MoSe$_2$ was mechanically exfoliated from bulk material onto a SiO$_2$ (285 nm)/Si substrate.

Experimental technique

In this work, degenerate femtosecond laser pump-probe technique has been employed to perform the transient measurements on ultrafast exciton/carrier dynamics under ambient conditions. Both pump and probe pulses were generated by a mode-locked Ti:Sapphire laser (Spectra Physics, Tsunami), with 80 MHz repetition rate and 800 nm central wavelength (resonant with *A* exciton of monolayer MoSe$_2$, see Fig. 1d). Both pump and probe beams were focused onto the same spot of the sample by a lens set, with the spot size about 80 μm in diameter. The reflected probe beam was collected by a photodetector connected to a lock-in amplifier. The sample structure and detection geometry are shown as the inset of Fig. 1a. The pulse width of both pump and probe pulses was around 100 fs at the sample surface. The polarizations of pump and probe beams were perpendicular to each other in order to eliminate the coherent artificial effect. PL measurement was conducted using Renishaw inVia Micro-Raman spectroscope with a 532 nm laser and a 50 × objective lens, at room-temperature in air. XPS spectra were acquired using an Omicron Multiprobe system and monochromatic Al Kα ($h\nu$ = 1486.7 eV) X-ray radiation source. The background pressure during measurements were kept below 3×10^{-10} mbar.

Data availability statement

The data that support the findings of this study are available from the corresponding author upon reasonable request.

AUTHOR CONTRIBUTIONS

Y.W. and K.C. conceived the original idea. K.C. performed all the ultrafast pump-probe experiments and data analysis. R.G. synthesized and prepared all the CVD samples. X. M. prepared the exfoliated sample. A.R. conducted the XPS experiments. J.K. conducted the PL and the static reflectivity measurements. F.H., S.M., and X.X. assisted the ultrafast pump-probe experiments and PL measurements. Y.W., J.F.L., D. A., and S.B. supervised all experiments. All authors took part in discussion on results and preparation of manuscript.

REFERENCES

1. Zhang, Y. et al. Direct observation of the transition from indirect to direct bandgap in atomically thin epitaxial MoSe$_2$. *Nat. Nanotechnol.* **9**, 111–115 (2014).
2. Mak, K. F., He, K., Shan, J. & Heinz, T. F. Control of valley polarization in monolayer MoS$_2$ by optical helicity. *Nat. Nanotechnol.* **7**, 494–498 (2012).
3. Mak, K. F. et al. Tightly bound trions in monolayer MoS$_2$. *Nat. Mater.* **12**, 207–211 (2013).
4. Mak, K. F. & Shan, J. Photonics and optoelectronics of 2D semiconductor transition metal dichalcogenides. *Nat. Photon.* **10**, 216–226 (2016).
5. Zhou, C. et al. Low voltage and high ON/OFF ratio field-effect transistors based on CVD MoS$_2$ and ultra high-k gate dielectric PZT. *Nanoscale* **7**, 8695–8700 (2015).
6. Withers, F. et al. Light-emitting diodes by band-structure engineering in van der Waals heterostructures. *Nat. Mater.* **14**, 301–306 (2015).

7. Perea-López, N. et al. CVD-grown monolayered MoS$_2$ as an effective photosensor operating at low-voltage. *2D Mater* **1**, 011004 (2014).

8. Wu, S. et al. Monolayer semiconductor nanocavity lasers with ultralow thresholds. *Nature* **520**, 69–72 (2015).

9. Gong, Z. et al. Magnetoelectric effects and valley-controlled spin quantum gates in transition metal dichalcogenide bilayers. *Nat. Commun.* **4**, 2053 (2013).

10. Lin, Z. et al. Defect engineering of two-dimensional transition metal dichalcogenides. *2D Mater* **3**, 022002 (2016).

11. Amani, M. et al. Near-unity photoluminescence quantum yield in MoS$_2$. *Science* **350**, 1065–1068 (2015).

12. Hong, J. et al. Exploring atomic defects in molybdenum disulphide monolayers. *Nat. Commun.* **6**, 6293 (2015).

13. Yuan, S., Roldán, R., Katsnelson, M. & Guinea, F. Effect of point defects on the optical and transport properties of MoS$_2$ and WS$_2$. *Phys. Rev. B* **90**, 041402 (2014).

14. Pandey, M. et al. Defect-tolerant monolayer transition metal dichalcogenides. *Nano. Lett.* **16**, 2234–2239 (2016).

15. Tongay, S. et al. Defects activated photoluminescence in two-dimensional semiconductors: interplay between bound, charged, and free excitons. *Sci. Rep.* **3**, 2657 (2013).

16. Neamen, D. A. *Semiconductor physics and devices* (McGraw-Hill Higher Education, 2003).

17. Wang, H., Zhang, C. & Rana, F. Ultrafast dynamics of defect-assisted electron–hole recombination in monolayer MoS$_2$. *Nano Lett.* **15**, 339–345 (2014).

18. Wang, H., Zhang, C. & Rana, F. Surface recombination limited lifetimes of photoexcited carriers in few-layer transition metal dichalcogenide MoS$_2$. *Nano Lett.* **15**, 8204–8210 (2015).

19. Shi, H. et al. Exciton dynamics in suspended monolayer and few-layer MoS$_2$ 2D crystals. *ACS Nano* **7**, 1072–1080 (2013).

20. Sun, D. et al. Observation of rapid exciton–exciton annihilation in monolayer molybdenum disulfide. *Nano Lett.* **14**, 5625–5629 (2014).

21. Liu, X. et al. An ultrafast terahertz probe of the transient evolution of the charged and neutral phase of photo-excited electron-hole gas in a monolayer semiconductor. *2D Mater* **3**, 014001 (2016).

22. Cunningham, P. D. et al. Charge trapping and exciton dynamics in large-area CVD grown MoS$_2$. *J. Phys. Chem. C* **120**, 5819–5826 (2016).

23. Docherty, C. J. et al. Ultrafast transient terahertz conductivity of monolayer MoS$_2$ and WSe$_2$ grown by chemical vapor deposition. *ACS Nano* **8**, 11147–11153 (2014).

24. Wang, H. et al. Fast exciton annihilation by capture of electrons or holes by defects via Auger scattering in monolayer metal dichalcogenides. *Phys. Rev. B* **91**, 165411 (2015).

25. Illarionov, Y. Y. et al. The role of charge trapping in MoS$_2$/SiO$_2$ and MoS$_2$/hBN field-effect transistors. *2D Mater.* **3**, 035004 (2016).

26. Katsidis, C. C. & Siapkas, D. I. General transfer-matrix method for optical multilayer systems with coherent, partially coherent, and incoherent interference. *Appl. Opt.* **41**, 3978–3987 (2002).

27. Wang, R. et al. Ultrafast and spatially resolved studies of charge carriers in atomically thin molybdenum disulfide. *Phys. Rev. B* **86**, 045406 (2012).

28. Hunsche, S., Leo, K., Kurz, H. & Köhler, K. Exciton absorption saturation by phase-space filling: influence of carrier temperature and density. *Phys. Rev. B* **49**, 16565 (1994).

29. Chemla, D., Miller, D., Smith, P., Gossard, A. & Wiegmann, W. Room temperature excitonic nonlinear absorption and refraction in GaAs/AlGaAs multiple quantum well structures. *IEEE J. Quant. Electron* **20**, 265–275 (1984).

30. Kumar, N. et al. Exciton-exciton annihilation in MoSe$_2$ monolayers. *Phys. Rev. B* **89**, 125427 (2014).

31. Cui, Q., Ceballos, F., Kumar, N. & Zhao, H. Transient absorption microscopy of monolayer and bulk WSe$_2$. *ACS Nano* **8**, 2970–2976 (2014).

32. Chernikov, A., Ruppert, C., Hill, H. M., Rigosi, A. F. & Heinz, T. F. Population inversion and giant bandgap renormalization in atomically thin WS$_2$ layers. *Nat. Photon.* **9**, 466–470 (2015).

33. Gong, T., Nighan, W. Jr & Fauchet, P. Hot-carrier Coulomb effects in GaAs investigated by femtosecond spectroscopy around the band edge. *Appl. Phys. Lett.* **57**, 2713–2715 (1990).

34. Steinhoff, A., Rosner, M., Jahnke, F., Wehling, T. & Gies, C. Influence of excited carriers on the optical and electronic properties of MoS$_2$. *Nano Lett.* **14**, 3743–3748 (2014).

35. Zhang, X.-X., You, Y., Zhao, S. Y. F. & Heinz, T. F. Experimental evidence for dark excitons in monolayer WSe$_2$. *Phys. Rev. Lett.* **115**, 257403 (2015).

36. Sim, S. et al. Exciton dynamics in atomically thin MoS$_2$: interexcitonic interaction and broadening kinetics. *Phys. Rev. B* **88**, 075434 (2013).

37. Siegner, U., Fluck, R., Zhang, G. & Keller, U. Ultrafast high-intensity nonlinear absorption dynamics in low-temperature grown gallium arsenide. *Appl. Phys. Lett.* **69**, 2566–2568 (1996).

38. Gupta, S. et al. Subpicosecond carrier lifetime in GaAs grown by molecular beam epitaxy at low temperatures. *Appl. Phys. Lett.* **59**, 3276–3278 (1991).

39. Kostoulas, Y., Waxer, L., Walmsley, I., Wicks, G. & Fauchet, P. Femtosecond carrier dynamics in low-temperature-grown indium phosphide. *Appl. Phys. Lett.* **66**, 1821–1823 (1995).

40. Kostoulas, Y., Ucer, K. B., Wicks, G. W. & Fauchet, P. M. Femtosecond carrier dynamics in low-temperature grown Ga$_{0.51}$In$_{0.49}$P. *Appl. Phys. Lett.* **67**, 3756–3758 (1995).

41. Chow, P. K. et al. Defect-induced photoluminescence in monolayer semiconducting transition metal dichalcogenides. *ACS Nano* **9**, 1520–1527 (2015).

42. Wu, Z. et al. Defects as a factor limiting carrier mobility in WSe$_2$: a spectroscopic investigation. *Nano Res.* **9**, 3622–3631 (2016).

43. Zafar, A. et al. Probing the intrinsic optical quality of CVD grown MoS$_2$. *Nano Res.* 1–10. doi:10.1007/s12274-016-1319-z (2016).

44. Attaccalite, C., Bockstedte, M., Marini, A., Rubio, A. & Wirtz, L. Coupling of excitons and defect states in boron-nitride nanostructures. *Phys. Rev. B* **83**, 144115 (2011).

45. Jeong, H. Y. et al. Visualizing point defects in transition-metal dichalcogenides using optical microscopy. *ACS Nano* **10**, 770–777 (2015).

46. Wang, X. et al. Chemical vapor deposition growth of crystalline monolayer MoSe$_2$. *ACS Nano* **8**, 5125–5131 (2014).

47. Köhler, A. Organic semiconductors: no more breaks for electrons. *Nat. Mater.* **11**, 836–837 (2012).

48. Ruzicka, B. A. et al. Spatially resolved pump-probe study of single-layer graphene produced by chemical vapor deposition [Invited]. *Opt. Mater. Express* **2**, 708–716 (2012).

49. Jin, Y. et al. A Van Der Waals homojunction: ideal p–n diode behavior in MoSe$_2$. *Adv. Mater.* **27**, 5534–5540 (2015).

50. Xia, B. et al. Zigzag-edge related ferromagnetism in MoSe$_2$ nanoflakes. *Phys. Chem. Chem. Phys.* **17**, 32505–32510 (2015).

51. Lee, C.-H. et al. Bi-axial grown amorphous MoS$_x$ bridged with oxygen on r-GO as a superior stable and efficient nonprecious catalyst for hydrogen evolution. *Sci. Rep.* **7**, 41190 (2017).

52. Vishwanath, S. et al. Comprehensive structural and optical characterization of MBE grown MoSe$_2$ on graphite, CaF$_2$ and graphene. *2D Mater* **2**, 024007 (2015).

53. Chianelli, R. et al. The reactivity of MoS$_2$ single crystal edge planes. *J. Catal.* **92**, 56–63 (1985).

54. Ghosh, R. et al. Large area chemical vapor deposition growth of monolayer MoSe$_2$ and its controlled sulfurization to MoS$_2$. *J. Mater. Res.* **31**, 917–922 (2016).